frontiers | Frontiers in Neuroimaging

TYPE Original Research
PUBLISHED 25 June 2024
DOI 10.3389/fnimg.2024.1336887

OPEN ACCESS

EDITED BY
Suyash P. Awate,
Indian Institute of Technology Bombay, India

REVIEWED BY
Yuchuan Zhuang,
AbbVie, United States
Vincent P. Ferrera,
Columbia University, United States

*CORRESPONDENCE
Mark Chiew
✉ mark.chiew@utoronto.ca

RECEIVED 11 November 2023
ACCEPTED 03 June 2024
PUBLISHED 25 June 2024

CITATION
Shahdloo M, Khalighinejad N, Priestley L, Rushworth M and Chiew M (2024) Dynamic off-resonance correction improves functional image analysis in fMRI of awake behaving non-human primates.
Front. Neuroimaging 3:1336887.
doi: 10.3389/fnimg.2024.1336887

Dynamic off-resonance correction improves functional image analysis in fMRI of awake behaving non-human primates

Mo Shahdloo[1], Nima Khalighinejad[1], Luke Priestley[1], Matthew Rushworth[1] and Mark Chiew[2,3,4]*

[1]Department of Experimental Psychology, Wellcome Centre for Integrative Neuroimaging, University of Oxford, Oxford, United Kingdom, [2]Nuffield Department of Clinical Neurosciences, Wellcome Centre for Integrative Neuroimaging, University of Oxford, Oxford, United Kingdom, [3]Physical Sciences, Sunnybrook Research Institute, Toronto, ON, Canada, [4]Medical Biophysics, University of Toronto, Toronto, ON, Canada

Introduction: Use of functional MRI in awake non-human primate (NHPs) has recently increased. Scanning animals while awake makes data collection possible in the absence of anesthetic modulation and with an extended range of possible experimental designs. Robust awake NHP imaging however is challenging due to the strong artifacts caused by time-varying off-resonance changes introduced by the animal's body motion. In this study, we sought to thoroughly investigate the effect of a newly proposed dynamic off-resonance correction method on brain activation estimates using extended awake NHP data.

Methods: We correct for dynamic B0 changes in reconstruction of highly accelerated simultaneous multi-slice EPI acquisitions by estimating and correcting for dynamic field perturbations. Functional MRI data were collected in four male rhesus monkeys performing a decision-making task in the scanner, and analyses of improvements in sensitivity and reliability were performed compared to conventional image reconstruction.

Results: Applying the correction resulted in reduced bias and improved temporal stability in the reconstructed time-series data. We found increased sensitivity to functional activation at the individual and group levels, as well as improved reliability of statistical parameter estimates.

Conclusions: Our results show significant improvements in image fidelity using our proposed correction strategy, as well as greatly enhanced and more reliable activation estimates in GLM analyses.

KEYWORDS

fMRI, non-human primate (NHP), raw data correction, off-resonance artifacts, simultaneous multi-slice

Introduction

Neuroanatomical and functional parallels between humans and non-human primates (NHPs) have made NHPs useful models for understanding the human brain (Andersen et al., 2019; Gray and Barnes, 2019; Picaud et al., 2019; Roberts and Clarke, 2019; Rudebeck et al., 2019). However, robust functional magnetic resonance imaging (fMRI) of the NHPs at high spatiotemporal resolution is challenging due a variety of factors, including the anatomical differences in brain size and head shape, behavioral differences in the scanner, and the specialized receive coils needed to facilitate NHP data acquisition (Autio et al., 2021; Friedrich et al., 2021; Hayashi et al., 2021; Yokoyama et al., 2021).

In order to capitalize on the statistical benefits that simultaneous multi-slice (SMS) imaging has provided in human imaging (Feinberg et al., 2010; Feinberg and Setsompop, 2013; Risk et al., 2021), recent studies have begun exploring the use of SMS acquisitions

with bespoke multichannel receive coils in imaging of anesthetized NHPs (Autio et al., 2020). Yet, the differing biological conditions between awake and anesthetized states could hinder utility of the results from the anesthetized NHP experiments when compared to the awake human state. This has led to a surge in awake NHP studies recently (Seah et al., 2014).

However, accelerated fMRI in awake behaving NHPs poses some unique challenges. Although the animal's head is typically mechanically stabilized in such experiments, motion in the behaving animal's body, hands, jaw, and facial musculature causes strong, fluctuating B0 field inhomogeneities within the brain (Pfeuffer et al., 2007; Goense et al., 2010). These dynamic field inhomogeneities cause not only considerable image distortion but invalidate the correspondence between the imaging data and calibration data used for SMS image reconstruction. This results in additional ghosting and residual aliasing artifacts (from other simultaneously excited slices) that cannot be corrected in post processing and can degrade image quality.

Multiple previous approaches have been proposed to estimate dynamic off-resonance in human neuroimaging using field sensors (Wilm et al., 2011; Kasper et al., 2015), multi-echo sequences (Visser et al., 2012; Dymerska et al., 2016; Zahneisen et al., 2017), or extra navigators (Splitthoff and Zaitsev, 2009; Wallace et al., 2020, 2021). But in the scope of awake NHP fMRI, these previous works are limited by requiring complicated additional hardware, compromising temporal resolution to accommodate multiple echoes, or requiring customized sequences. Recently, we proposed a method to correct for these dynamic B0 changes (Shahdloo et al., 2022) by using the reference navigator data which are often available in most standard echo planar imaging (EPI) sequences used for fMRI data acquisition (Figure 1A). While we had shown improvements in conventional image fidelity metrics, the impact of this off-resonance correction method has yet to be quantified on downstream estimates of brain activation.

Here, we aim to validate this off-resonance correction method using GLM analysis of task-fMRI data from 40 awake behaving NHP scans across 4 animals. Our results show significant reductions in image bias and variance, as well as improvements in temporal signal to noise ratio (tSNR) and detected activations across the brain.

Methods

We recently proposed to correct for dynamic B0 changes in reconstruction of highly accelerated SMS acquisitions by estimating and correcting for dynamic field perturbations (Shahdloo et al., 2022). This method uses navigator data acquired at every time-point for Nyquist ghost correction, and the GRAPPA-based operator weights trained on a calibration scan to estimate a first-order dynamic field perturbation at each time-point relative to the calibration scan. This can be interpreted as estimating a net translation in k-space due to the field perturbation. Then, this estimate is used to transform the acquired data to enhance consistency with the calibration data for a ghost- and alias-free SMS image reconstruction (Figure 1B). The NHP fMRI experiments detailed here are used to quantify the impact of this off-resonance correction method on downstream estimates of brain activation.

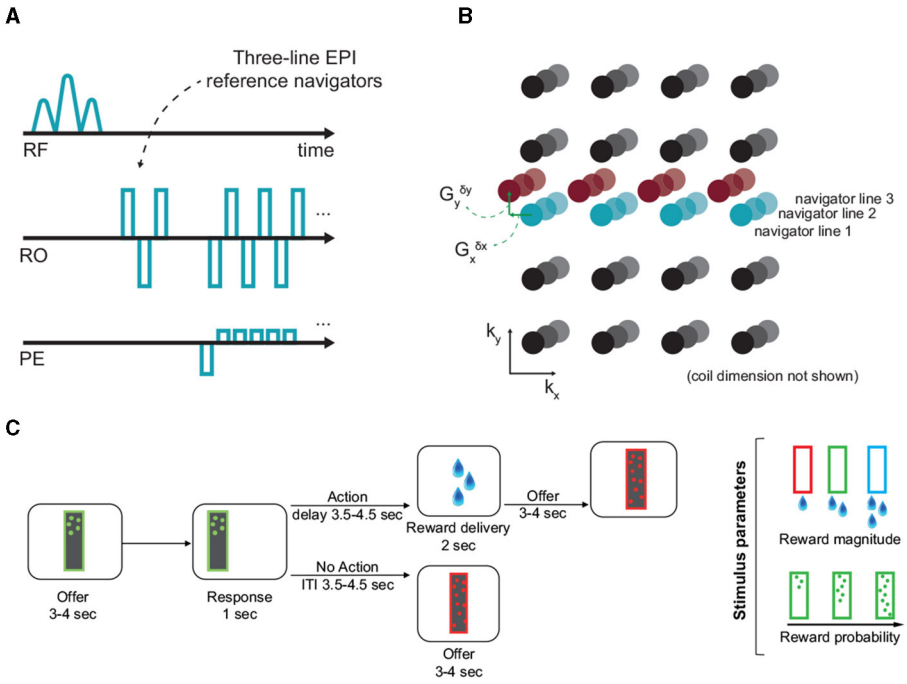

FIGURE 1
Off-resonance correction, and the experimental paradigm. **(A, B)** EPI reference navigators in each frame are compared to a reference frame to estimate the dynamic linear off-resonance. These estimates are then used to correct the imaging data (Shahdloo et al., 2022). **(C)** This off-resonance correction method was validated in a decision-making task in awake NHPs, where the animals decide to act based on the number and color of dots appearing on the screen, respond by touching a pad, and receive a liquid reward based on the response. The experimental paradigm involves a wide range of body motion, as well as irregular events.

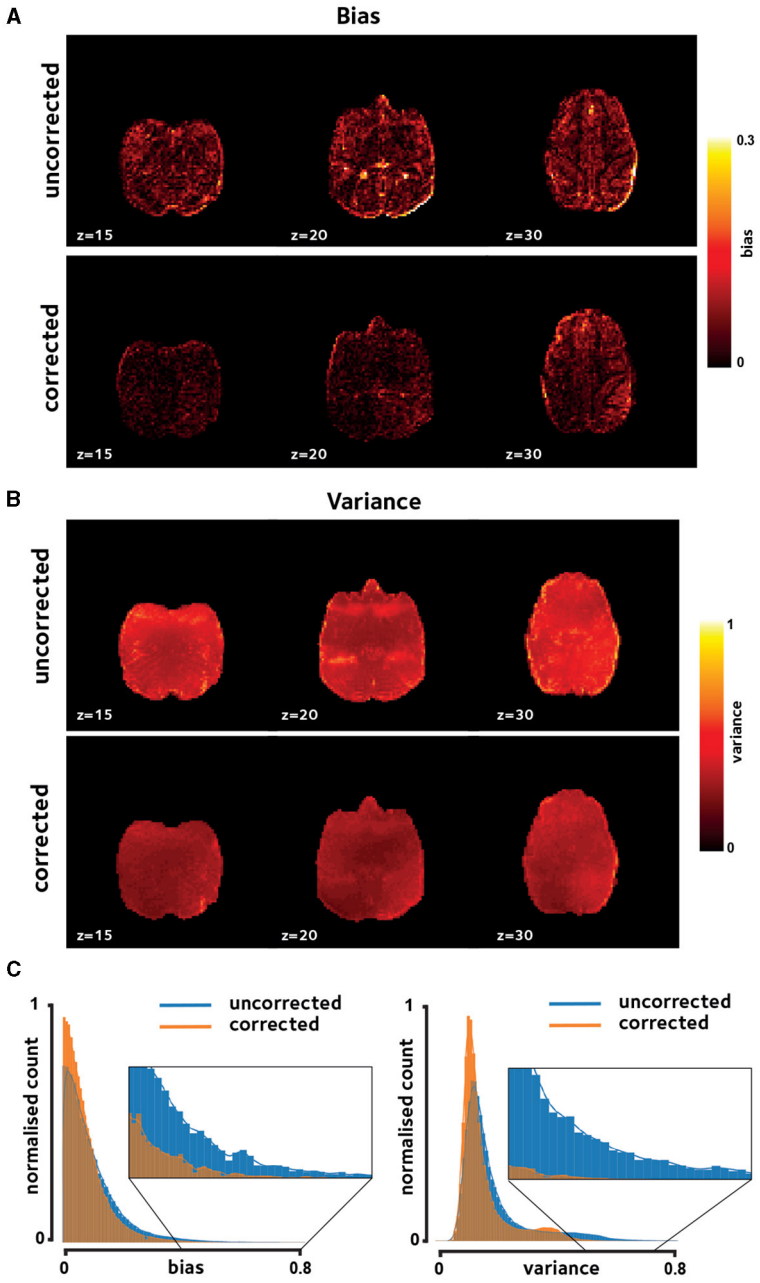

FIGURE 2
Reconstruction fidelity. Improvements in image quality were assessed using **(A)** reconstruction bias and **(B)** temporal variation, shown for a representative session. Off-resonance correction reduces the reconstruction bias and variance across the brain. **(C)** Histogram of these measures taken over brain voxels and pooled across sessions in the same representative monkey verifies the observed reduction in bias and variance.

Behavioral task

In vivo 2D fMRI data from four male rhesus monkeys were collected (weight 14.1–16.8 kg, 6–8 years of age) while they were performing a decision-making task. All procedures were conducted under licenses from the United Kingdom (UK) Home Office in accordance with The UK Animals Act 1986 (Scientific Procedures) and with the European Union guidelines (EU Directive 2010/63/EU).

The task was developed from the one originally used in our recent studies (Khalighinejad et al., 2020, 2022). At the beginning of each trial a frame (8 × 26 cm) appeared on the center of the screen. The frame contained different number of dots. The color and number of dots within the frame represented the magnitude and probability of potential reward, respectively. After 3–4 s the frame moved to either the left or right side of the screen. Animals could respond (within 1 s) by touching a custom-made infrared touch sensor, on the side corresponding to the image. The

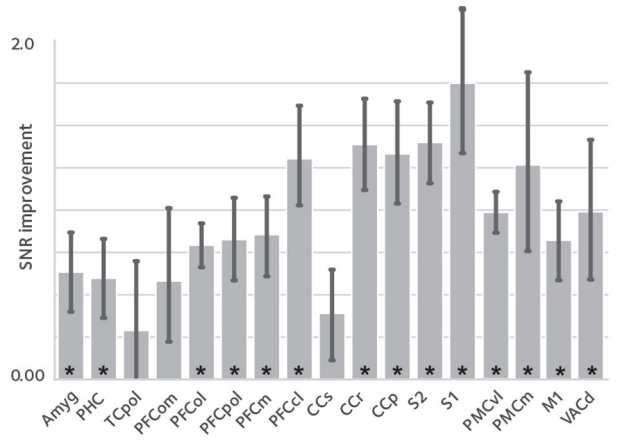

FIGURE 3
tSNR enhancement. To assess the effect of image quality improvements on the fMRI time series, temporal signal to noise ratio (tSNR) was compared between reconstructions, in anatomical ROIs [mean ± sem; asterisks denote statistical significance at q(FDR) < 0.05]. tSNR is significantly improved in most of the studied ROIs that cover the whole brain.

probability of getting a reward and the drops of juice received depended on the number and color of the dots, respectively (Figure 1C). If they responded, they were offered drops of juice or no juice, based on reward probability on that trial. There was a delay of 3.5–4.5 s between response and outcome (action-outcome delay). If rewarded, drops of juice were delivered by a spout placed near the animal's mouth. If they did not respond, the next offer appeared after a 3.5–4.5 s intertrial interval (ITI). Reward magnitude and probability of the offer changed from one trial to another.

Imaging protocol and reconstruction

The animals were head-fixed in sphinx position in an MRI-compatible chair in a clinical 3T scanner. Data were acquired using a 15-channel bespoke receive coil (Rapid Biomedical, Berlin, Germany), using the CMRR multi-band GRE-EPI sequence (Moeller et al., 2010; Setsompop et al., 2012) with parameters: TE/TR = 25.4/1,282 ms, FA = 63°, FOV = 120 mm, 1.25 mm isotropic resolution, 42 slices, MB = 2, in-plane acceleration factor R = 2. Data from 10 runs were collected from each of the four animals, each containing 1,213–1,364 volumes. Raw data were separately reconstructed using the online reconstruction provided as part of the CMRR multi-band EPI sequence package and using our proposed GRAPPA-operator based dynamic off-resonance corrected reconstruction method. Single-band reference data and fully sampled calibration data were acquired along with the functional data as separate parts of the imaging sequence. Standard Nyquist ghost correction and dynamic zeroth-order B0 correction were applied on all reconstructions prior to off-resonance estimation and correction (Shahdloo et al., 2022).

Preprocessing

Data preprocessing was performed using tools from FMRIB Software Library (FSL; Jenkinson et al., 2012), Advanced Normalization Tools (ANTs;27/10/2023 22:53:00; Tustison et al., 2014), and the Magnetic Resonance Comparative Anatomy Toolbox (MrCat; Mars et al., 2016). A mean EPI reference image was created for each session, to which all volumes were non-linearly registered on a slice-by-slice basis along the phase-encoding direction to correct for time-varying distortions in the main magnetic field due to body and limb motion. The aligned and distortion-corrected functional images were then non-linearly registered to each animal's high-resolution structural images (binarizing threshold = 0.1). A group specific template was constructed by registering each animal's structural image to the CARET macaque F99 space (Kolster et al., 2009). Finally, the functional images were temporally filtered (high-pass temporal filtering, 3-dB cutoff of 100 s) and spatially smoothed (Gaussian spatial smoothing, full-width half maximum of 3 mm). The same preprocessing parameters and pipelines were used for the uncorrected and off-resonance corrected reconstructions.

Quantification and statistical analysis

Quantifying image quality

To validate the effect of dynamic off-resonance correction on image quality before preprocessing, the mean image difference compared to the single-band reference (bias) and the temporal coefficient of variation (variance) were calculated. To do this, the raw data were reconstructed using the vendor-provided reconstruction on the scanner, and with our proposed offline reconstruction that incorporates off-resonance correction. The single-band reference was reconstructed using the vendor-provided reconstruction on the scanner.

To assess the image quality improvement with finer granularity, temporal signal to noise ratio (tSNR) values in anatomical regions of interest (ROIs) were compared between the uncorrected and corrected reconstructions, where tSNR was taken as the ratio of the signal mean to standard deviation in each voxel. To enable pooling of tSNRs across animals and sessions, the data were mapped from the functional space onto the standard F99 space. To create anatomical ROIs, voxel masks were created for each ROI in the F99 standard space using the Rhesus Monkey Brain Atlas (Paxinos, 2009). Masks were then transformed from the standard space to each participant's structural space by applying a standard-to-structural warp field and from structural to functional space by applying a structural-to-functional affine matrix. Transformed masks were thresholded, binarised and were dilated by one voxel. tSNR values were averaged across voxels within anatomical ROI boundaries.

Whole-brain functional analysis

Whole-brain statistical analyses were performed at two-levels as implemented in FSL FEAT. At the first level, a univariate general linear model (GLM) was fit to the preprocessed data

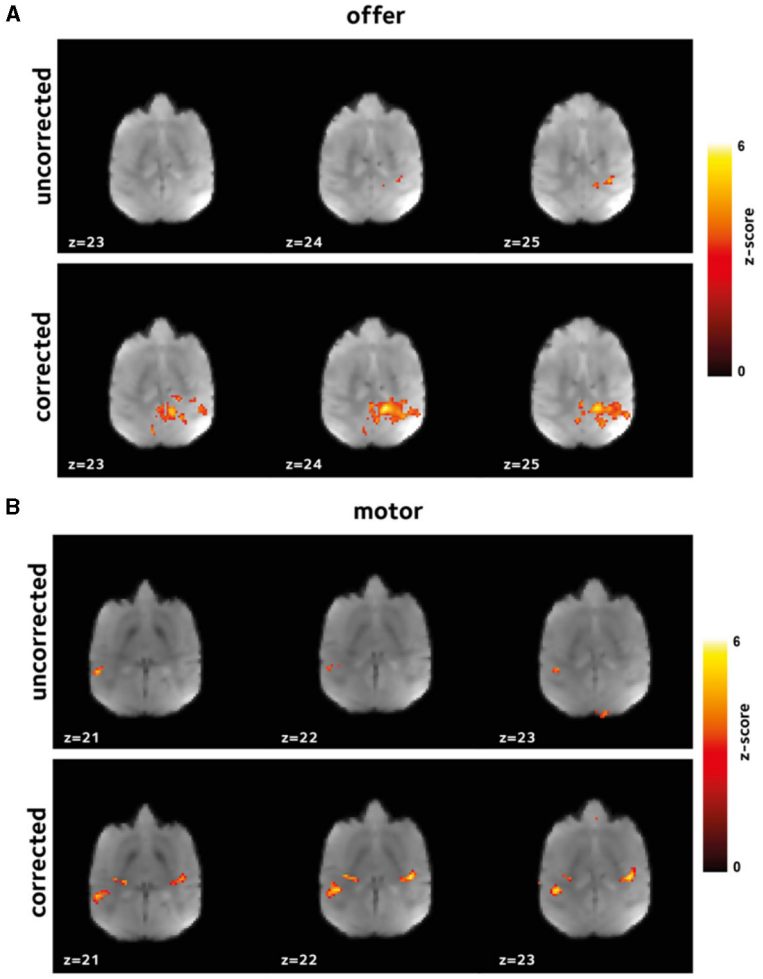

FIGURE 4
Improvement in first level GLM analysis. GLM models were fit to the data in each session to identify voxels that were activated **(A)** by *offer*, and **(B)** by the *motor_response* variables. Thresholded z-scores in a representative session are shown. Functional signal quality is improved using the off-resonance correction, as reflected by the larger number of voxels passing the threshold.

in each animal. The parameter estimates across sessions were then combined in a second-level mixed-effects analysis (FLAME 1+2), taking scanning sessions as random effect. The results were cluster-corrected with the voxel inclusion threshold of $z = 3.1$ and cluster significance threshold of $p = 0.05$. The data were pre-whitened to account for temporal autocorrelations.

The first-level analyses looked for voxels where the response reflected parametric variation in BOLD response according to the following GLM model.

$$BOLD = \beta_0 + \beta_1 offer + \beta_2 action\_onset + \beta_3 motor\_response + \beta_4 outcome$$

where *BOLD* is a column vector containing the times-series data for a given voxel. *offer* is an unmodulated regressor representing the main effect of stimulus presentation (all event amplitudes set to one). *action_onset* is also an unmodulated regressor representing the go-cue (frame moving to either the left or right side of the screen). *motor_response* is a binary regressor representing response (pressing on the touch sensor) vs. no-response. *outcome* is an unmodulated regressor representing the main effect of outcome. Regressors were modeled as a boxcar function with constant duration of 0.1 s convoluted with a hemodynamic response function (HRF) specific for monkey brains. Regressor 1 was time-locked to the onset of the trial (presentation of the offer). Regressors 2 and 3 were time-locked to the go-cue onset. Regressor 4 was time-locked to the onset of the reward outcome phase.

Reliability analysis

Reliability of the fMRI analyses using the uncorrected and corrected reconstructions were assessed and compared. In a 10-fold cross validation, experimental sessions were pooled across subjects and randomly divided into two groups. The second level analysis was then performed on each of the groups. Thresholded *z*-score values in anatomical ROIs were compared between the

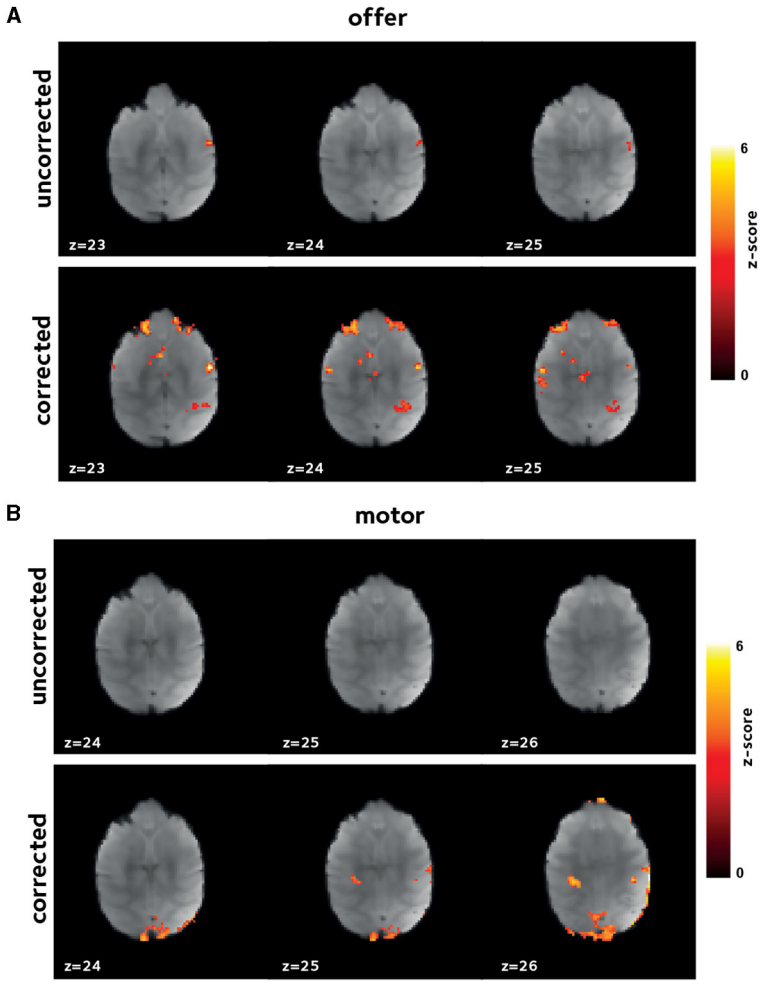

FIGURE 5
Improvement in first level GLM analysis. Thresholded z-score maps in a representative session from a second animal showing activated voxels **(A)** by *offer*, and **(B)** by the *motor_response* variables. The improvements in functional signal quality are consistent across animals.

two groups and reliability was measured as the linear correlation coefficient between the z-score values. Furthermore, to ensure that the applied off-resonance correction has not introduced bias in the activation baseline, mean z-score values across ROI voxels were compared. Baseline bias was taken as the absolute difference between the mean z-score in each ROI between the two groups.

Results

Qualitative inspection of Figures 2A, B shows reduced bias and temporal variance due to off-resonance correction in a session in a representative monkey, indicating increased reconstruction fidelity. Notably, presence of dynamic off-resonance had led to reconstruction artifacts in the original data that were not addressed using the conventional preprocessing pipeline that was applied. These artifacts are most prominent in the anterior and posterior regions, where half-FOV aliasing artifacts are most prominent. Figure 2C shows the histogram of the bias and variance values across brain voxels in the same monkey, pooled across sessions. Distribution of bias and variance in the corrected reconstruction is skewed toward zero, indicating larger number of voxels with low bias and variance compared to the uncorrected reconstruction.

Enhanced temporal signal stability would be expected as a result of the reduction in reconstruction variance. tSNR difference between corrected reconstruction compared to the uncorrected reconstruction was calculated and averaged in anatomical ROIs, shown in Figure 3. tSNR is significantly increased in the studied ROIs [q(FDR) < 0.05, non-significant in TCpol, PFCom, and CCS].

Here, we have hypothesized that the reduced bias and variance, and enhanced temporal signal stability should reflect the reduction in artifacts, and hence, increased statistical power in the downstream GLM analyses. This enhancement is expected to be manifested in larger estimates of regression coefficients with potentially larger number of voxels having estimates regression coefficients above any

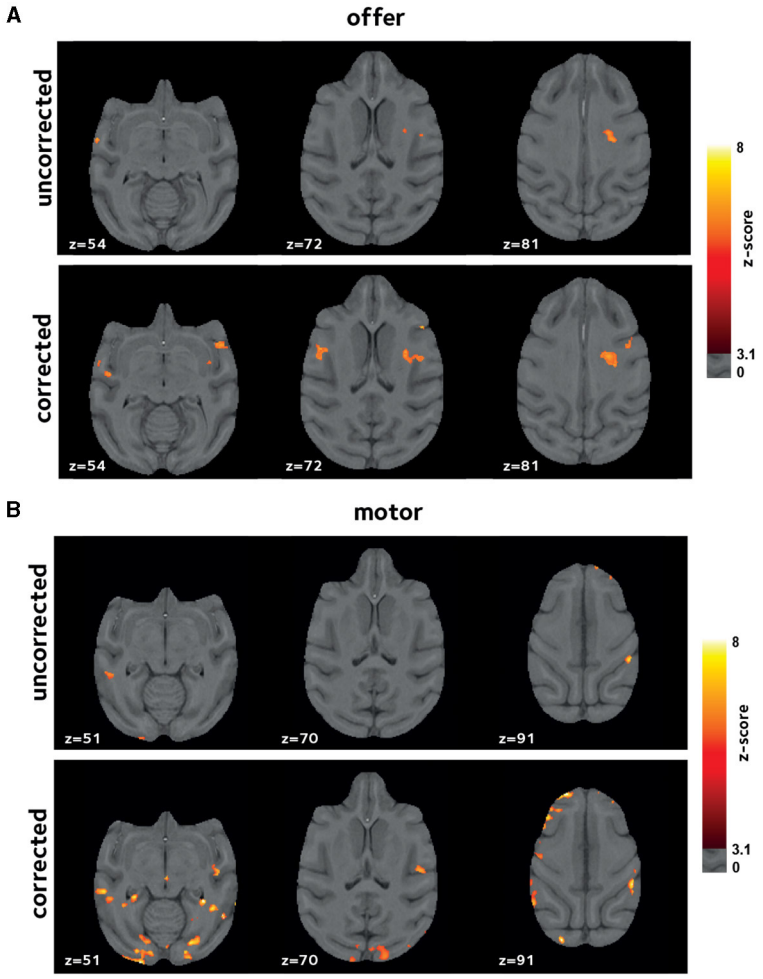

FIGURE 6
Improvements in second-level analysis. A second-level mixed-effects analysis was performed taking scanning sessions as random effect. Thresholded z-score maps are shown indicating activated voxels **(A)** by *offer*, and **(B)** by the *motor_response* variables. The off-resonance correction significantly improves the results of the higher-level GLM analysis.

certain set threshold. To test this hypothesis, we performed first-level analysis. Figures 4, 5 show thresholded z-score maps in representative sessions in two animals. Representative maps relating to the *offer* and *motor_response* regressors are shown, as they could elicit responses in widely differing brain regions. At a set threshold, the proposed off-resonance correction leads to a larger number of activated voxels, and larger effect sizes which is noticeable even at the level of single sessions.

Inherent inter-subject variablity at the single-session level could lead to high variation among sessions. Thus, to account for this effect in the comparing the uncorrected and corrected reconstructions, we also investigated the results of a second-level mixed-effects analysis, taking scanning sessions as random effect. Figure 6 shows the 2nd-level z-score maps for the same regressors shown in Figures 4, 5 (thresholded at $z = 3.1$). Reaffirming the results from the first-level analysis, off-resonance correction leads to a larger number of voxels surviving the threshold (Tables 1, 2). Abbreviations used for brain ROIs are defined in Table 3.

The experimental procedure used here results in sessions with varying time lengths. Thus, we investigated the reliability of the second-level analysis by correlating the second-level z-score maps between two random splits of the sessions pooled across subjects, via a cross-validation procedure. Figure 7 shows the second-level reliability in anatomical ROIs. Off-resonance corrected reconstruction leads to more reliable results in ROIs with activated voxels.

Discussion

Accelerated awake NHP fMRI entails unique challenges compared to human fMRI, one of the main ones being reconstruction artifacts due to dynamic off-resonance changes. In head-posted animals, motion in body parts could cause strong field changes that introduce artifacts and distort the images

TABLE 1 Activated voxels by *offer*.

	Uncorrected		Corrected	
	N voxels	Max *z*	*N* voxels	Max *z*
Amyg	130	3.77	1,535	4.26
PHC	326	3.22	287	3.51
TCpol	0	-	416	3.43
CCr	0	-	215	3.28
CCp	209	3.12	701	4.07
S1	354	3.54	613	4.47
S2	107	3.57	887	4.14
PCm	20	3.30	69	3.62
PMCvl	444	3.19	3,947	4.92
PMCm	0	-	1,127	3.92
VACd	105	3.11	374	3.38

To quantify the improvements in the higher-level analysis, the number of activated voxels by the *offer* variable were counted in each ROI. The off-resonance correction improves the number of activated voxels, as well as the peak z-scores across the brain.

TABLE 2 Activated voxels by the *motor_response*.

	Uncorrected		Corrected	
	N voxels	Max *z*	*N* voxels	Max *z*
Amyg	0	-	862	3.80
TCpol	0	-	640	3.85
CCp	160	3.78	191	4.58
S1	178	3.32	479	4.56
S2	80	3.63	907	3.69
PMCvl	3,753	5.76	555	3.68
PMCm	0	-	297	3.92
M1	0	-	254	3.78

To quantify the improvements in the higher-level analysis, the number of activated voxels by *motor_response* variable were counted in each ROI. Consistent with Table 1, the off-resonance correction improves the number of activated voxels, as well as the peak z-scores across the brain.

in a way that cannot be corrected in preprocessing. There is therefore a need for approaches for artifact suppression and distortion correction during image reconstruction. Recently, we proposed a method to achieve this using the navigator data that is already collected during the fMRI acquisition. Here, we used a large amount of awake NHP data from a physically demanding and dynamic decision-making experiment to investigate the efficacy of this off-resonance correction. Our results show that improvements in image fidelity and temporal stability lead to improved estimates of brain activation. Moreover, the method studied here relies only on the navigator data acquired using conventional accelerated acquisition sequences. Thus, applying this off-resonance correction retrospectively to previously acquired scans is possible and can improve fMRI analyses if raw imaging data are available.

TABLE 3 ROI abbreviations.

Abbreviation	ROI name
Amyg	Amygdala
PHC	Parahippocampal cortex
TCpol	Pole of temporal cortex
CCr	Retrosplenial cingulate gyrus
CCp	Posterior cingulate gyrus
S1	Primary somatosensory cortex
S2	Secondary somatosensory cortex
PCm	Medial parietal cortex
PMCvl	Ventrolateral premotor cortex
PMCm	Medial premotor cortex
VACd	Visual anterior cortex, dorsal part
M1	Primary motor cortex

ROI abbreviations referred to in Tables 1, 2, according to Rhesus Monkey Brain Atlas (Paxinos, 2009).

The off-resonance correction method used here assumes first-order spatial off-resonance perturbations that have been shown to be a good approximation in imaging headposted NHPs (Pfeuffer et al., 2007). One limitation of this correction is that the accuracy of the first-order approximation can potentially suffer from extreme body motion. The experimental paradigm used here entails long runs where animals perform choices by pressing on a touch sensor and receive liquid rewards, each of which involve a large range of motion in body parts. The results show that the linear correction can significantly improve parameter estimates across the brain. However, highly dynamic experimental setups may benefit from extra non-linear preprocessing steps to reduce the residual artifacts and distortion.

It should also be noted that the correction performance depends heavily on the capability of the receive coil in parallel imaging. The data used here were acquired using a bespoke NHP coil with relatively good spatial coverage. However, the improvements might be hindered if an unsuitable coil had been used for data collection.

Conclusion

In conclusion, the method validated here enables more robust and reliable NHP imaging in accelerated acquisitions that leads to significantly improved functional analysis results in awake NHP studies.

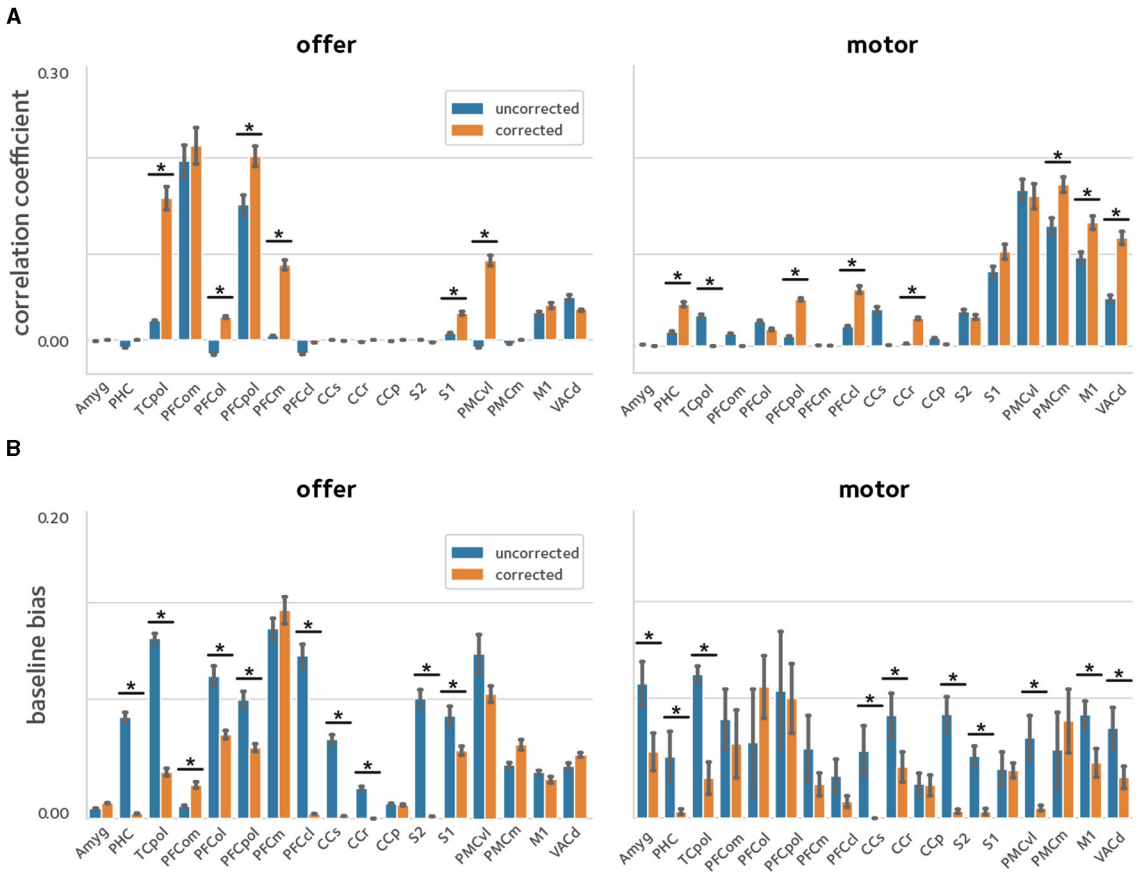

FIGURE 7
Reliability of activation estimates. To quantify the improvements in reliability of the estimated activations, a cross-validation procedure was used were the sessions pooled across animals were randomly divided in two and models were fit in each sub-group separately. Reliability was quantified by taking the **(A)** correlation, and **(B)** baseline bias between the estimates in the two sub-groups [asterisks denote statistical significance at q(FDR) < 0.05]. The off-resonance correction significantly improves the reliability of activation estimates across the brain.

Data availability statement

Raw data cannot be shared due to legal/ethical reasons, however, minimal data can be shared by the corresponding author upon request - requests should be directed to mark.chiew@utoronto.ca.

Ethics statement

The animal study was approved by United Kingdom (UK) Home Office. The study was conducted in accordance with the local legislation and institutional requirements.

Author contributions

MS: Writing – review & editing, Writing – original draft, Visualization, Validation, Software, Resources, Methodology, Investigation, Data curation. NK: Writing – review & editing, Validation, Resources, Investigation, Funding acquisition. LP: Writing – review & editing, Resources, Data curation. MR: Writing – review & editing, Validation, Resources, Funding acquisition. MC: Writing – review & editing, Writing – original draft, Validation, Supervision, Resources, Project administration, Methodology, Funding acquisition, Data curation, Conceptualization.

Funding

The author(s) declare financial support was received for the research, authorship, and/or publication of this article. The Wellcome Center for Integrative Neuroimaging was supported by core funding from the Wellcome Trust (203139/Z/16/Z). NK was funded by BBSRC Discovery Fellowship (BB/W008947/1). MR was supported by BBSRC fellowship (BB/W003392/1) and Wellcome Trust award (221794/Z/20/Z). MC was supported by the Canada Research Chairs Program.

Conflict of interest

The authors declare that the research was conducted in the absence of any commercial or financial relationships that could be construed as a potential conflict of interest.

Publisher's note

References

Andersen, R. A., Aflalo, T., and Kellis, S. (2019). From thought to action: the brain-machine interface in posterior parietal cortex. *Proc. Natl. Acad. Sci. U. S. A.* 116, 26274–26279. doi: 10.1073/pnas.1902276116

Autio, J. A., Glasser, M. F., Ose, T., Donahue, C. J., Bastiani, M., Ohno, M., et al. (2020). Towards HCP-Style macaque connectomes: 24-Channel 3T multi-array coil, MRI sequences and preprocessing. *NeuroImage* 215:116800. doi: 10.1016/j.neuroimage.2020.116800

Autio, J. A., Zhu, Q., Li, X., Glasser, M. F., Schwiedrzik, C. M., Fair, D. A., et al. (2021). Minimal specifications for non-human primate MRI: challenges in standardizing and harmonizing data collection. *NeuroImage* 236:118082. doi: 10.1016/j.neuroimage.2021.118082

Dymerska, B., Poser, B. A., Bogner, W., Visser, E., Eckstein, K., Cardoso, P., et al. (2016). Correcting dynamic distortions in 7T echo planar imaging using a jittered echo time sequence. *Magn. Reson. Med.* 76, 1388–1399. doi: 10.1002/mrm.26018

Feinberg, D. A., Moeller, S., Smith, S. M., Auerbach, E., Ramanna, S., Glasser, M. F., et al. (2010). Multiplexed echo planar imaging for sub-second whole brain fMRI and fast diffusion imaging. *PLoS ONE* 5:e15710. doi: 10.1371/journal.pone.0015710

Feinberg, D. A., and Setsompop, K. (2013). Ultra-fast MRI of the human brain with simultaneous multi-slice imaging. *J. Magn. Reson.* 229, 90–100. doi: 10.1016/j.jmr.2013.02.002

Friedrich, P., Forkel, S. J., Amiez, C., Balsters, J. H., Coulon, O., Fan, L., et al. (2021). Imaging evolution of the primate brain: the next frontier? *NeuroImage* 228:117685. doi: 10.1016/j.neuroimage.2020.117685

Goense, J. B. M., Whittingstall, K., and Logothetis, N. K. (2010). Functional magnetic resonance imaging of awake behaving macaques. *Methods* 50, 178–188. doi: 10.1016/j.ymeth.2009.08.003

Gray, D. T., and Barnes, C. A. (2019). Experiments in macaque monkeys provide critical insights into age-associated changes in cognitive and sensory function. *Proc. Natl. Acad. Sci. U. S. A.* 116, 26247–26254. doi: 10.1073/pnas.1902279116

Hayashi, T., Hou, Y., Glasser, M. F., Autio, J. A., Knoblauch, K., Inoue-Murayama, M., et al. (2021). The nonhuman primate neuroimaging and neuroanatomy project. *NeuroImage* 229:117726. doi: 10.1016/j.neuroimage.2021.117726

Jenkinson, M., Beckmann, C. F., Behrens, T. E. J., Woolrich, M. W., and Smith, S. M. (2012). FSL. *NeuroImage* 62, 782–790. doi: 10.1016/j.neuroimage.2011.09.015

Kasper, L., Bollmann, S., Vannesjo, S. J., Gross, S., Haeberlin, M., Dietrich, B. E., et al. (2015). Monitoring, analysis, and correction of magnetic field fluctuations in echo planar imaging time series. *Magn. Reson. Med.* 74, 396–409. doi: 10.1002/mrm.25407

Khalighinejad, N., Bongioanni, A., Verhagen, L., Folloni, D., Attali, D., Aubry, J.-F., et al. (2020). A basal forebrain-cingulate circuit in macaques decides it is time to act. *Neuron* 105, 370–384.e8. doi: 10.1016/j.neuron.2019.10.030

Khalighinejad, N., Manohar, S., Husain, M., and Rushworth, M. F. S. (2022). Complementary roles of serotonergic and cholinergic systems in decisions about when to act. *Curr. Biol.* 32, 1150–1162.e7. doi: 10.1016/j.cub.2022.01.042

Kolster, H., Mandeville, J. B., Arsenault, J. T., Ekstrom, L. B., Wald, L. L., and Vanduffel, W. (2009). Visual field map clusters in macaque extrastriate visual cortex. *J. Neurosci.* 29, 7031–7039. doi: 10.1523/JNEUROSCI.0518-09.2009

Mars, R. B., Verhagen, L., Gladwin, T. E., Neubert, F. X., Sallet, J., and Rushworth, M. F. S. (2016). Comparing brains by matching connectivity profiles. *Neurosci. Biobehav. Rev.* 60, 90–97. doi: 10.1016/j.neubiorev.2015.10.008

Moeller, S., Yacoub, E., Olman, C. A., Auerbach, E., Strupp, J., Harel, N., et al. (2010). Multiband multislice GE-EPI at 7 tesla, with 16-fold acceleration using partial parallel imaging with application to high spatial and temporal whole-brain FMRI. *Magn. Reson. Med.* 63, 1144–1153. doi: 10.1002/mrm.22361

Paxinos, G. (2009). *The Rhesus Monkey Brain: in Stereotaxic Coordinates, 2 Edn*. Amsterdam; Heidelberg: Elsevier; Academic Press.

Pfeuffer, J., Shmuel, A., Keliris, G. A., Steudel, T., Merkle, H., and Logothetis, N. K. (2007). Functional MR imaging in the awake monkey: effects of motion on dynamic off-resonance and processing strategies. *Magn. Reson. Imag. Proc. Int. Sch. Magnet. Reson. Brain Funct.* 25, 869–882. doi: 10.1016/j.mri.2007.03.002

Picaud, S., Dalkara, D., Marazova, K., Goureau, O., Roska, B., and Sahel, J.-A. (2019). The primate model for understanding and restoring vision. *Proc. Natl. Acad. Sci. U. S. A.* 116, 26280–26287. doi: 10.1073/pnas.1902292116

Risk, B. B., Murden, R. J., Wu, J., Nebel, M. B., Venkataraman, A., Zhang, Z., et al. (2021). Which multiband factor should you choose for your resting-state fMRI study? *NeuroImage* 234:117965. doi: 10.1016/j.neuroimage.2021.117965

Roberts, A. C., and Clarke, H. F. (2019). Why we need nonhuman primates to study the role of ventromedial prefrontal cortex in the regulation of threat- and reward-elicited responses. *Proc. Natl. Acad. Sci. U. S. A.* 116, 26297–26304. doi: 10.1073/pnas.1902288116

Rudebeck, P. H., Rich, E. L., and Mayberg, H. S. (2019). From bed to bench side: reverse translation to optimize neuromodulation for mood disorders. *Proc. Natl. Acad. Sci. U. S. A.* 116, 26288–26296. doi: 10.1073/pnas.1902287116

Seah, S., Asad, A. B. A., Baumgartner, R., Feng, D., Williams, D. S., Manigbas, E., et al. (2014). Investigation of cross-species translatability of pharmacological MRI in awake nonhuman primate—a Buprenorphine Challenge Study. *PLoS ONE* 9:e110432. doi: 10.1371/journal.pone.0110432

Setsompop, K., Gagoski, B. A., Polimeni, J. R., Witzel, T., Wedeen, V. J., and Wald, L. L. (2012). Blipped-controlled aliasing in parallel imaging for simultaneous multislice echo planar imaging with reduced g-factor penalty. *Magn. Reson. Med.* 67, 1210–1224. doi: 10.1002/mrm.23097

Shahdloo, M., Schüffelgen, U., Papp, D., Miller, K. L., and Chiew, M. (2022). Model-based dynamic off-resonance correction for improved accelerated fMRI in awake behaving nonhuman primates. *Magn. Reson. Med.* 2022:mrm.29167. doi: 10.1002/mrm.29167

Splitthoff, D. N., and Zaitsev, M. (2009). SENSE shimming (SSH): a fast approach for determining B0 field inhomogeneities using sensitivity coding. *Magn. Reson. Med.* 62, 1319–1325. doi: 10.1002/mrm.22083

Tustison, N. J., Cook, P. A., Klein, A., Song, G., Das, S. R., Duda, J. T., et al. (2014). Large-scale evaluation of ANTs and FreeSurfer cortical thickness measurements. *Neuroimage* 99, 166–179. doi: 10.1016/j.neuroimage.2014.05.044

Visser, E., Poser, B. A., Barth, M., and Zwiers, M. P. (2012). Reference-free unwarping of EPI data using dynamic off-resonance correction with multiecho acquisition (DOCMA). *Magn. Reson. Med.* 68, 1247–1254. doi: 10.1002/mrm.24119

Wallace, T. E., Afacan, O., Kober, T., and Warfield, S. K. (2020). Rapid measurement and correction of spatiotemporal B0 field changes using FID navigators and a multi-channel reference image. *Magn. Reson. Med.* 83, 575–589. doi: 10.1002/mrm.27957

Wallace, T. E., Polimeni, J. R., Stockmann, J. P., Hoge, W. S., Kober, T., Warfield, S. K., et al. (2021). Dynamic distortion correction for functional MRI using FID navigators. *Magn. Reson. Med.* 85, 1294–1307. doi: 10.1002/mrm.28505

Wilm, B. J., Barmet, C., Pavan, M., and Pruessmann, K. P. (2011). Higher order reconstruction for MRI in the presence of spatiotemporal field perturbations. *Magn. Reson. Med.* 65, 1690–1701. doi: 10.1002/mrm.22767

Yokoyama, C., Autio, J. A., Ikeda, T., Sallet, J., Mars, R. B., Van Essen, D. C., et al. (2021). Comparative connectomics of the primate social brain. *NeuroImage* 245:118693. doi: 10.1016/j.neuroimage.2021.118693

Zahneisen, B., Aksoy, M., Maclaren, J., Wuerslin, C., and Bammer, R. (2017). Extended hybrid-space SENSE for EPI: off-resonance and eddy current corrected joint interleaved blip-up/down reconstruction. *Neuroimage* 153, 97–108. doi: 10.1016/j.neuroimage.2017.03.052